ChemComm

Electrochemical Behaviour of Uranium at a Tripolyphosphate Modified ITO Electrode

Journal:	*ChemComm*
Manuscript ID	CC-COM-07-2021-003877.R2
Article Type:	Communication

Chemical Communications

COMMUNICATION

Electrochemical Behaviour of Uranium at a Tripolyphosphate Modified ITO Electrode

Received 17th July 2021,
Accepted 00th September 2021

DOI: 10.1039/x0xx00000x

Xiangyang Hou,[a] Jeffrey R. McLachlan,[a] and Christopher J. Dares[a,*]

UO_2^{2+} binds to the surface of a tripolyphosphate modified mesoporous indium tin-doped oxide electrode (*nano*ITO|P_3). Electrochemical studies reveal that *n*ITO|P_3 electrodes catalyze the 2-electron interconversion between UO_2^{2+} and U^{4+} with the P_3-ligand assisting in the rate-limiting proton-coupled reduction of U(V) to U(IV), based on the kinetic isotope effect (1.8). Product composition between *n*ITO|P_3(U^{4+}) and surface adsorbed UO_2 can be controled by adjusting the proton concentration and/or scan rate in voltammograms. These studies with uranium suggest that *n*ITO|P_3 electrodes are good candidates for redox transformations with other actinides including neptunium, plutonium, and americium.

In acidic solutions, the most stable form of uranium is UO_2^{2+}. This linear di-cation features hexavalent uranium and uranyl-oxygen bonds which are formally triple bonds.[1] These strong bonds make it a challenge to labilize the oxygen atoms. The 1-electron reduction of UO_2^{2+} produces UO_2^{+}, which can disproportionate to form U^{4+} and UO_2^{2+} (Scheme 1).[2] Stabilization of the pentavalent species can be enhanced through cation-cation interactions including the formation of $UO_2^{2+}\cdots UO_2^{+}$ associated complexes.[3] Further proton-coupled reduction to the tetravalent state involves destruction of the uranyl cation.

Scheme 1. Latimer diagrams of U and Am in 1 M acid. Potentials are in V vs. SHE.

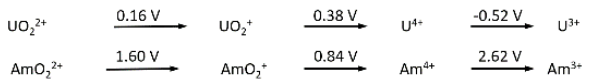

The linear actinyl cation (AnO_2^{n+}, n = 1 or 2) is featured for other penta- and hexavalent actinides found in used nuclear fuel including Np, Pu, and Am. Reprocessing used nuclear material including actinides requires precise oxidation state control.[4] While U, Np, and Pu oxidation states can be adjusted and maintained with various chemical oxidants or reductants (including U(IV)). Am exists as Am(III) and is a challenge to oxidize to the hexavalent state given the high Am(IV/III) potential (2.62 V vs. SHE).[5] Reprocessing Am with the other actinyl species would decrease fuel cycle costs and increase storage and disposition options.[6] Concentrated phosphoric acid solutions have been used to generate Am(IV), and feature stable Am(IV) phosphate complexes.[7] The solubility of these same complexes is low hindering solution studies, while coordination site saturation inhibits the formation of actinyl species. Further oxidation in acidic media to AmO_2^{+} or AmO_2^{2+} is also a challenge because of the proton-coupled electron transfer (PCET) required to form the americyl cation. Ligands can be used to facilitate these redox events,[8] and using the principle of microscopic reversibility, a ligand able to labilize the An—O_{yl} bonds will also be able to facilitate their formation. Our work in actinide redox chemistry has included the development of ligand modified electrodes (LMEs). These include a mesoporous thin film of a conductive metal oxide such as indium tin-doped oxide (ITO) surface functionalized with a ligand capable of binding actinides.[9] LMEs with N-donor ligands have yet to quantitatively oxidize Am(III) to Am(VI), and result in a mixture of Am(V) and Am(VI).[10] While Am(V) is a weaker oxidant than Am(IV), slow sequential electron transfer hinders further oxidation. To that end, we have prepared a tripolyphosphate functionalized electrode (*n*ITO|P_3) (Figure 1), which can perform the 2-electron reduction of UO_2^{2+} to U^{4+} and UO_2 with minimal UO_2^{+} generated as an intermediate at potentials as mild as -0.25 V in 0.1 M $HClO_4$. These surrogate studies provide evidence that our *n*ITO|P_3 electrodes will act as good electrocatalysts for the oxidation of Am(III) to Am(VI).

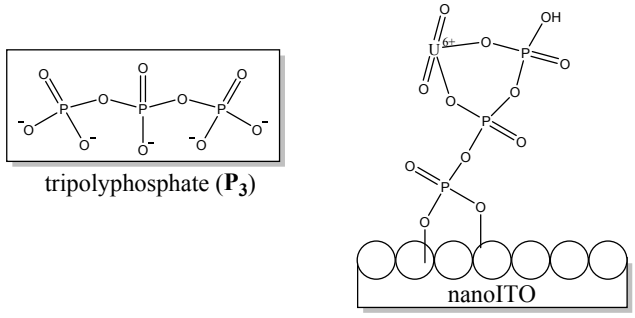

Figure 1. Structure of tripolyphosphate (P_3), and depiction of the binding of UO_2^{2+} at a *n*ITO|P_3 electrode.

Except for uranyl acetate and uranyl nitrate, which contained depleted uranium, and were donated by FIU Environmental Health and Safety from an existing stockpile, all chemicals and solvents were purchased as reagent grade or better from Fisher Scientific and used as received. Fluorine-doped tin oxide (FTO)

[a] *Florida International University, Department of Chemistry and Biochemistry, 11200 SW 8th St. Miami, FL 33199 USA*
† email: cdares@fiu.edu
Electronic Supplementary Information (ESI) available: An include experimental details and supporting electrochemical data. See DOI: 10.1039/x0xx00000x

sputtered coated glass was purchased from Hartford Glass, Inc. *n*ITO electrodes were fabricated according to published procedures.[17] *n*ITO|P_3 electrodes were prepared by soaking a *n*ITO electrode in a 2 mM solution of sodium tripolyphosphate for 24 h and then rinsed with fresh 0.1 M $HClO_4$ before use. Instrument details are included in the supplementary information.

X-ray photoelectron (XPS) spectra confirm the tripolyphosphate ligand (P_3) at the surface of *n*ITO|P_3 electrodes (Figure S6) with a P 2p signal at 133.7 eV. Cyclic voltammograms (CVs) of 1 mM UO_2^{2+} in 0.1 M $HClO_4$ at a bare *n*ITO and a *n*ITO|P_3 electrode are shown in Figure 2. At the bare *n*ITO electrode, a single U(VI) reduction is observed at -0.25 V vs. SCE, with a corresponding oxidation event at -0.14 V. This couple is ascribed to the diffusion-limited U(VI/V) redox couple (Figure S11). At potentials beyond the UO_2^{2+} reduction peak, further reduction of UO_2^{2+} occurs with possible slow proton reduction. The weak broad oxidation event at ca. 0.4 V is attributed to the oxidation of U(IV) oxides (mainly UO_2 though it may include U(IV) hydroxides). This assignment is consistent with bulk electrolysis of a 1 mM UO_2^{2+} solution in 0.1 M $HClO_4$ using a bare *n*ITO electrode with an applied potential of -0.40 V for 18 h (Figure S12). The first scan of the bare *n*ITO electrode in fresh 0.1 M $HClO_4$ after electrolysis features a broad oxidation at ~0.45 V that becomes negligible after the first scan, while the reduction of UO_2^{2+} is subsequently observed at -0.25 V. The presence of uranium oxide at the surface is confirmed by XPS with the inclusion of U 4f signals at 383.05 eV (Figure S2 and S7).[11] The oxide layer formed during electrolysis is weakly adsorbed to the surface and is stripped from the surface upon oxidation. Oxidation of U(V) is not observed for the first scan but is after subsequent scans (*vide infra*).

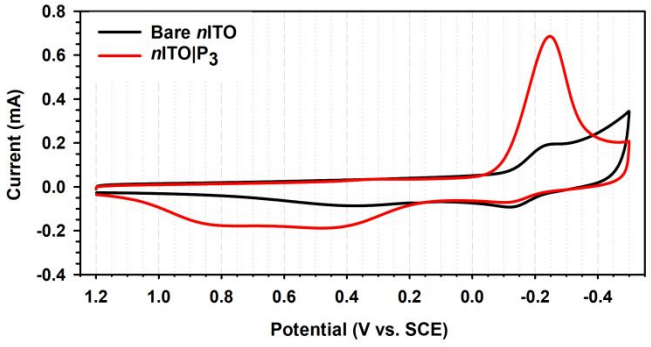

Figure 2. CVs at 50 mV/s starting at 1.2 V of 1 mM UO_2^{2+} at bare *n*ITO electrode (**black**) and *n*ITO|P_3 electrode (**red**) in 0.1 M $HClO_4$.

CVs of a *n*ITO|P_3 electrode in 0.1 M $HClO_4$ with 1 mM UO_2^{2+}, feature a current enhancement of the UO_2^{2+} reduction at -0.25 V, a weak UO_2^{+} oxidation at -0.14 V, and two significant and broad oxidation events at +0.45 V and +0.80 V assigned to the oxidation of UO_2 and U^{4+} respectively (Figure 2).[12] These redox events are diffusion-limited due to free dissociation of uranium (Figure S13).[13] The oxidation of UO_2^{+} is observed from the stabilization imparted by the formation of cation-cation interaction species including $UO_2^{2+}\cdots UO_2^{+}$ (Figure S14). Scan rate dependent linear sweep voltammetry studies in 0.1 M $HClO_4$ show that the composition of U(IV) as U^{4+} and UO_2 varies as a function of scan rate (Figure S15). At slow scan rates, UO_2 is favoured, since the U^{4+} generated has more time to hydrolyze to UO_2. At faster scan rates, the proportion of U^{4+} relative to UO_2 increases to a point where it becomes independent of scan rate.

Controlled potential electrolysis of a 0.1 M $HClO_4$ solution with 10 mM UO_2^{2+} at -0.40 V with a *n*ITO|P_3 electrode in a 2-compartment cell with concurrent spectroscopic monitoring features the generation of U^{4+} with a Faradaic efficiency of 88 % and a first-order rate constant for the appearance of U^{4+} of 5.4×10^{-3} min^{-1} (Figure S17). This is superior to a bare *n*ITO electrode under the same conditions which has a Faradaic efficiency of 68 % and a first-order rate constant for U^{4+} appearance of 2.8×10^{-3} min^{-1} (Figure S16).

Soaking a *n*ITO|P_3 electrode in a 1 mM UO_2^{2+} solution of 0.1 M $HClO_4$ for 10 min followed by rinsing 3-times with fresh 0.1 M $HClO_4$ reveals that UO_2^{2+} is bound to the tripolyphosphate ligand with a surface coverage of 8.5 nmol/cm^2 (Figure S19). Surface coverage was determined using eq. 1, where Γ is the surface coverage in mol/cm^2, Q is the charge passed during the oxidation at +0.97 V, n is the number of electrons transferred (2.0), F is the Faraday constant (96,485 C/mol), and A is the area of the electrode (1.00 cm^2). Negligible UO_2^{2+} binding to bare *n*ITO is observed.

$$\Gamma = Q/nFA \quad (1)$$

XPS of *n*ITO|P_3 soaked in UO_2^{2+} confirms U(VI) at the surface with U *4f* signals at 382.45 eV (Figure S8).[11] The relative atomic ratio between uranium and phosphorous at the surface measured by XPS is 1:3, or one uranium atom per P_3 ligand (Table S4). UO_2^{2+} dissociates from the *n*ITO|P_3 electrodes in fresh 0.1 M $HClO_4$ solutions with a first order rate constant of 9.7×10^{-4} s^{-1}, while U^{4+} dissociates with a rate constant of 11×10^{-4} s^{-1} (Figures S20-22). Scan rate dependent studies of freshly UO_2^{2+} loaded *n*ITO|P_3 electrodes show a linear dependence between the peak current associated with UO_2^{2+} reduction and scan rate, highlighting the surface nature of the reduction event (Figure S23). Soaking a *n*ITO|P_3 electrode in a 1 mM solution of electrochemically generated U^{4+} in 0.1 M $HClO_4$, results in binding of U^{4+} to the *n*ITO|P_3 electrode with the same surface coverage as with UO_2^{2+} (Figure 3).[14] Starting from 0 V with an anodic scan direction, the CV of the U^{4+} soaked *n*ITO|P_3 electrode in fresh 0.1 M $HClO_4$ after rinsing first features the 2-electron oxidation of bound U^{4+} to UO_2^{2+} at +0.97 V, with no evidence of UO_2^{+} (*vide infra*). A single reduction at -0.25 V is attributed to the re-reduction of the P_3-bound electrochemically generated UO_2^{2+} (Figure S24). The XPS spectra of the U^{4+} soaked *n*ITO P_3 electrode features U *4f* signals at 383.05 eV (Figure S9), a 0.60 eV shift to higher energy relative to the UO_2^{2+} soaked *n*ITO|P_3 electrode, and is indicative of tetravalent uranium.[11]

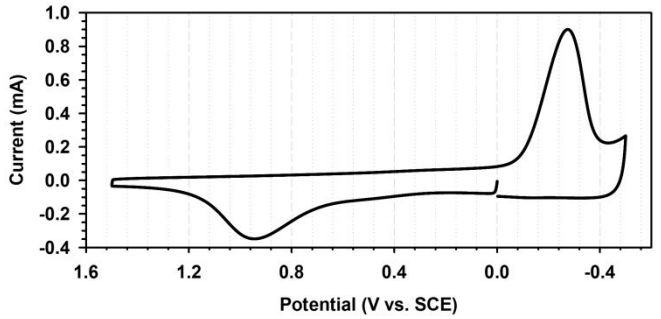

Figure 3. CV at 50mV/s starting at 0 V of *n*ITO|P_3 electrode in 0.1 M $HClO_4$ after soaking in 1 mM U^{4+} for 10 min.

The absence of additional UO_2^{2+} in solution prevents the formation of a $UO_2^{2+}\cdots UO_2^{+}$ cation-cation interactions and explains the absence of a UO_2^{+} oxidation. The large separation between the U^{4+} oxidation and UO_2^{2+} reduction (ΔE = 1.22 V) highlights the challenges associated with the reversible formation and destruction of the uranyl structure. Successive cycling of uranium-soaked *n*ITO|P_3 electrodes in fresh 0.1 M $HClO_4$ results in a minor reductive shoulder at ~+0.3 V which is indicative of a minor amount of UO_2^{+} generated from the oxidation of U^{4+}. This assignment was confirmed by performing partial bulk reduction of a 1 mM UO_2^{2+} solution at -0.2 V in 0.1 M $HClO_4$ with a Pt coil electrode to generate a solution that includes UO_2^{2+}, U^{4+} and UO_2^{+} (Figure S25). CVs of the resultant solution feature a more prominent UO_2^{+} reduction to U(IV) at +0.26 V (Figure 4). Square-wave voltammetry of this partially reduced solution more clearly shows the reduction of U(V) (Figure S26).

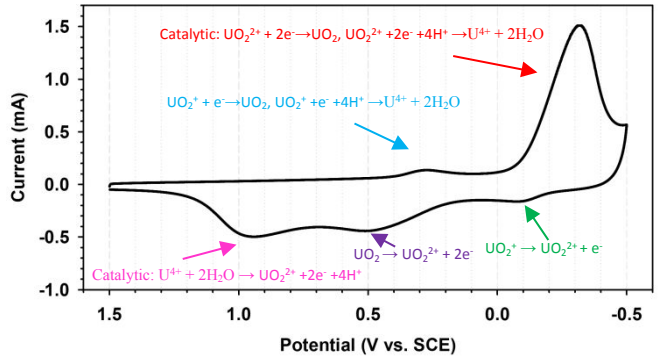

Figure 4. CV starting at 1.5 V of *n*ITO|P_3 electrode in 0.1 M $HClO_4$ acquired at 50 mV/s in a 1 mM U solution containing UO_2^{2+}, UO_2^{+}, and U^{4+} from reduction at -0.20 V (Figure S15).

To understand the effect proton concentration has on the electrochemical behaviour of uranium at *n*ITO|P_3 electrodes, the proton concentration was varied. In 3 M $HClO_4$, at bare *n*ITO with 1 mM UO_2^{2+}, an increase in reductive current with E < -0.1 V is observed with a possible UO_2^{+} re-oxidation at -0.05 V (Figure S27). This behaviour is similar to what has been reported at a Pt electrode in 0.1 M $HClO_4$.[12, 15] With a *n*ITO|P_3 electrode, a peak for the UO_2^{2+} reduction to U^{4+} is observed at -0.19 V, while again a minor UO_2^{+} oxidation is observed at +0.05 V. In contrast to studies in 0.1 M $HClO_4$, in 3 M $HClO_4$, UO_2 oxidation is not observed, and solely oxidation of U^{4+} is observed (E_{ox} = 1.10 V).[12] Adjusting the CV windows of *n*ITO|P_3 electrodes soaked in 1 mM UO_2^{2+} for 10 min highlights features of the electrochemical behaviour of uranium in 3 M acid at *n*ITO|P_3 (Figure S28). Cycling between 0 V and 1.4 V do not feature any U-based redox events since only U(VI) is bound to the P_3 ligand (Figure S29). Performing a full CV scan starting at 1.4 V to -0.4 V and ending at 0.6 V features a prominent UO_2^{2+} reduction at -0.25 V. This feature is less intense on a subsequent cycle which scans between +0.6 V and -0.4 V. This is because the U^{4+} formed from the previous full scan was not re-oxidized and now occupies some of the spaces on the P_3 ligand, and therefore less UO_2^{2+} present. A final full scan reproduces the previous full scan with a full intensity UO_2^{2+} reduction event. These multiple cycles confirm that U^{4+} binds to P_3 even at these high acidity solutions. Varying the proton concentration from 0.1 M to 3 M using a constant ionic strength of 3 M through the addition of $NaClO_4$ highlights the proton dependence of the observed U-based redox couples using *n*ITO|P_3 in the presence of 1 mM UO_2^{2+} (Figure S31) and after soaking in 1 mM UO_2^{2+} for 10 min (Figure S32). The reduction ascribed to eq. 5 at *n*ITO|P_3 is expected to have a pH dependent slope of -118 mV/pH unit if it adheres to the Nernst equation (eq. 2).

$$E = E^o - \frac{Rt}{nF}\ln\frac{[Red]}{[Ox]} - 0.059\frac{n_{H^+}}{n_{e^-}}pH \quad (2)$$

$$UO_2^{2+} + 1e^- \rightarrow UO_2^{+} \quad (3)$$

$$UO_2^{+} + 1e^- + 4H^+ \rightarrow U^{4+} + 2H_2O \quad (4)$$

$$UO_2^{2+} + 2e^- + 4H^+ \rightarrow U^{4+} + 2H_2O \quad (5)$$

$$U^{4+} + 2H_2O \rightarrow UO_2^{+} + 1e^- + 4H^+ \quad (6)$$

$$UO_2^{+} \rightarrow UO_2^{2+} + 1e^- \quad (7)$$

$$U^{4+} + 2H_2O \rightarrow UO_2^{2+} + 2e^- + 4H^+ \quad (8)$$

Assuming that the proton activity is equal to its concentration, the pH dependence of *n*ITO|P_3 electrodes soaked in UO_2^{2+} have a slope of -88 mV/pH unit, which suggests an electron-proton ratio between 1:1 and 1:2 and indicates that both the 1-electron (eq. 3 and 4) and 2-electron (eq. 5) reductions of UO_2^{2+} are occurring. The oxidation event which we ascribed to the oxidation of U^{4+} to UO_2^{2+} has a pH dependent slope of -102 mV/pH at *n*ITO|P_3 and is within expectations to assign the peak to the 2-electron oxidation of *n*ITO|P_3 bound U^{4+} to bound UO_2^{2+}(eq. 8). The oxidation of UO_2^{+} (eq. 7) observed in solutions containing UO_2^{2+} is independent of proton concentration (as expected).

The shape of the catalytic UO_2^{2+} reduction at *n*ITO|P_3 makes it possible to perform the foot-of-the-wave analysis (FOTW analysis) developed by Savéant and co-workers to determine the related catalytic rate constants.[16] This includes using eq. 9 and eq. 10 to derive eq. 11 for our heterogenous system. In eq. 9-11, i is the experimentally measured current during catalysis, i_p is the current associated with the reduction of the substrate in the absence of the catalyst, Γ is the surface coverage of P_3 bound UO_2^{2+}, F is the Faraday constant, R is the ideal gas constant, T is the temperature, A is the electrode area, E is the applied potential, E^o is the reduction potential for UO_2^{2+}, v is the scan rate, and k_{obs} is the observed rate constant associated with the catalytic process.

$$i_p = \frac{FA^2\Gamma}{4RT} \quad (9)$$

$$i = \frac{2FA\Gamma}{1 + \exp\left[\frac{F}{RT}(E - E^o)\right]} k_{obs} \quad (10)$$

$$\frac{i}{i_p} = \frac{8RT}{Fv\left\{1+\exp\left[\frac{F}{RT}(E-E^o)\right]\right\}} k_{obs} \quad (11)$$

In 0.1 M $HClO_4$, k_{obs} for the reduction of UO_2^{2+} at *n*ITO|P_3 can be determined from the slope of the rising region of eq. 5 where interferences from catalyst inhibition from bound U^{4+} are minimized. Varying the concentration of UO_2^{2+} from 0.01 mM to 0.5 mM (Figure S33), we observe a linear increase in k_{obs} (Figure 5) from 1 s^{-1} to 5 s^{-1}. The H/D kinetic isotope effect (KIE) for UO_2^{2+} reduction at *n*ITO|P_3 was determined by comparing the k_{obs} value determined from FOTW analysis in 0.1 M $HClO_4$ and $DClO_4$ (Figure S34). A KIE value of 1.8 from these experiments indicates the rate limiting step in the reduction of UO_2^{2+} at *n*ITO|P_3 involves proton transfer. This is consistent with expectations of a fast reduction of UO_2^{2+} to UO_2^{+} followed by a rate limiting reduction of UO_2^{+} to U^{4+} (eq. 12 and 13). The P_3 ligand is clearly involved in this rate limiting step as no catalysis is observed at bare *n*ITO.

$$nITO|P_3\left(UO_2^{2+}\right) + 1e^- \rightarrow nITO|P_3\left(UO_2^{+}\right) \quad \text{(fast)} \quad (12)$$

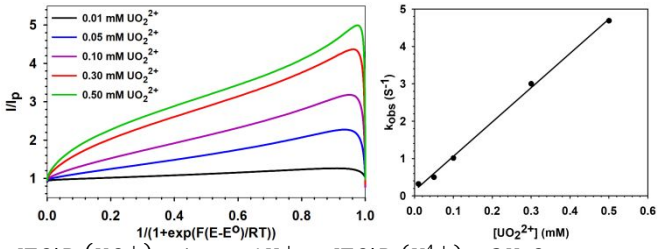

$$nITO|P_3\left(UO_2^{+}\right) + 1e^- + 4H^+ \rightarrow nITO|P_3\left(U^{4+}\right) + 2H_2O \quad \text{(slow)} \quad (13)$$

Figure 5. FOTW analysis of the reduction of UO_2^{2+} at a *n*ITO|P_3 electrode in 0.1 M $HClO_4$. First order rate constants (k_{obs}) values were determined from slopes of the rising region.

In summary, *n*ITO|P_3 electrodes effectively facilitate both the 2-electron reduction of UO_2^{2+} and the 2-electron oxidation of U^{4+} in acidic solutions and feature good chemical reversibility in these conditions. The rate-determining step in the decomposition or formation of the uranyl cation involves PCET. FOTW analysis for the reduction of UO_2^{2+} indicates it is first order in uranyl concentration. Given that reduction of UO_2^{2+} to U(IV) is observed at *n*ITO|P_3 electrodes at proton concentrations up to 3 M, while this is not observed at bare *n*ITO or *n*ITO|PO_4 (Figure S20), it can be concluded that the P_3 ligand is involved in this critical PCET event. The redox behaviours of uranium uncovered here provide a reference for the redox behaviour of transuranic elements with a special interest in Am(III) which may feature electrocatalytic oxidation to AmO_2^{+} or AmO_2^{2+}, especially in concentrated acid solutions where AmO_2^{+} can disproportionate to form AmO_2^{2+}.

This research was supported by the U.S. Department of Energy (US-DOE), Office of Nuclear Energy through the Nuclear Energy University Program (NEUP) under award number DE-NE0008539, and the Center for Actinide Science and funded by the US-DOE, Office of Science, Basic Energy Sciences, under Award Number DE-SC0016568. J.R.M was supported by the U.S. Nuclear Regulatory Commission with a Graduate Student Fellowship (NRC-HQ-84-14-G-0038).

Conflicts of interest

There are no conflicts to declare.

Notes and references

1. A. Kiernicki, J. J.; Cladis, D. P.; Fanwick, P. E.; Zeller, M.; Bart, S. C., *J. Am. Chem. Soc.* 2015, ***137***, 11115−11125; B. Denning, R. G., *J. Phys. Chem. A* 2007, ***111***, 4125-4143; C. Cowie, B. E.; Purkis, J. M.; Austin, J.; Love, J. B.; Arnold, P. L., *Chem Rev* 2019, ***119***, (18), 10595-10637.

2. A. Nocton, G.; Horeglad, P.; Vetere, V.; Pecaut, J.; Dubois, L.; Maldivi, P.; Edelstein, N. M.; Mazzanti, M., *J. Am. Chem. Soc.* 2010, ***132***, 495–508; B. Teyar, B.; Boucenina, S.; Belkhiri, L.; Le Guennic, B.; Boucekkine, A.; Mazzanti, M., *Inorg Chem* 2019, ***58***, (15), 10097-10110.

3. A. Ekstrom, A., *Inorg. Chem.* 1974, ***13***, (9), 2237-2241; B. Newton, T. W.; Baker, F. B., *Inorg. Chem.* 1965, ***4***, (8), 1166-1170; C. Madic, C.; Guillaume, B.; Morisseau, J. C.; Moulin, J. P., *J. Inorg. Nucl. Chem.* 1979, ***41***, 1027-1031.

4. Lumetta, G. J.; Allred, J. R.; Bryan, S. A.; Hall, G. B.; Levitskaia, T. G.; Lines, A. M.; Sinkov, S. I., *Sep. Sci. Tech.* 2019, ***54***, (12), 1977-1984.

5. McCann, K.; Mincher, B. J.; Schmitt, N. C.; Braley, J. C., *Ind. Eng. Chem. Res.* 2017, ***56***, (22), 6515-6519.

6. Gelis, A. V.; Kozak, P.; Breshears, A. T.; Brown, M. A.; Launiere, C.; Campbell, E. L.; Hall, G. B.; Levitskaia, T. G.; Holfeltz, V. E.; Lumetta, G. J., *Sci. Rep.* 2019, ***9***, (1), 12842.

7. Myasoedov, B. F.; Mikhailov, V. M.; Lebedev, I. A.; Koiro, O. E.; Frenkel, V. Y., *Radiochem. Radioanal. Lett.* 1973, ***14***, 17.

8. A. Chiang, M.-H.; Soderholm, L.; Antonio, Mark R., *Eur. J. Inorg. Chem.* 2003, ***2003***, 2929-2936; B. Bell, N. L.; Shaw, B.; Arnold, P. L.; Love, J. B., *J. Am. Chem. Soc.* 2018, ***140***, (9), 3378-3384.

9. Dares, C. J.; Lapides, A. M.; Mincher, B. J.; Meyer, T. J., *Science* 2015, ***350***, (6261), 652-655.

10. Lopez, M. J.; Sheridan, M. V.; McLachlan, J. R.; Grimes, T. S.; Dares, C. J., *Chem. Commun.* 2019, ***55***, (28), 4035-4038.

11. Ilton, E. S.; Bagus, P. S., *Surf. Inter. Anal.* 2011, ***43***, (13), 1549-1560.

12. Ikeda-Ohno, A.; Hennig, C.; Tsushima, S.; Scheinost, A. C.; Bernhard, G.; Yaita, T., *Inorg. Chem.* 2009, ***48***, (15), 7201-7210.

13. Agarwal, R.; Sharma, M. K., *Inorg. Chem.* 2018, ***57***, (17), 10984-10992.

14. Eller, P. G.; Penneman, R. A., *J. Less. Comm. Met.* 1987, ***127***, 19-33.

15. Mizuguchi, K.; Park, Y.-Y.; Tomiyasu, H.; Ikeda, Y., *J. Nucl. Sci. Tech.* 1993, ***30***, (6), 542-548.

16. Costentin, C.; Drouet, S.; Robert, M.; Savéant, J.-M., *J. Amer. Chem. Soc.* 2012, ***134***, (27), 11235-11242.

17. Sheridan, M. V.; McLachlan, J. R.; Gonzalez-Moya, J. R.; Cortes-Medina, N. D.; Dares, C. J., *ACS Appl Mater Interfaces* 2021, ***13***, (33), 40127-40133.